Upstream entrainment in numerical simulations of spatially evolving round jets

Pradeep C. Babu and Krishnan Mahesh[a)]
Aerospace Engineering and Mechanics, University of Minnesota, 107 Akerman Hall, Minneapolis, Minnesota 55455

(Received 19 March 2004; accepted 8 June 2004; published online 1 September 2004)

Direct numerical simulation is used to study the effect of entrainment near the inflow nozzle on spatially evolving round jets. Inflow entrainment is obtained by providing a buffer region upstream of the inflow nozzle. Simulations are performed at Reynolds numbers of 300 (laminar) and 2400 (turbulent), respectively. Simulations without the inflow buffer are contrasted to those with the buffer region. The potential core is seen to close earlier in the presence of inflow entrainment. As a result, near-field turbulent intensities and pressure fluctuations on the jet centerline are noticeably affected. It is suggested that inflow entrainment results in an effective co-flow, whose effect on the volumetric flow rate near the inflow nozzle is appreciable for both laminar and turbulent jets. When plotted in similarity variables, the far-field solutions with and without inflow entrainment agree well with each other, and experiment. The results suggest the importance of allowing for inflow entrainment in simulations of turbulent jets, particularly for studies where near-field behavior is important. © *2004 American Institute of Physics*. [DOI: 10.1063/1.1780548]

I. INTRODUCTION

Turbulent jets have been studied for a variety of reasons, e.g., self-similarity,[1–3] jet control,[4,5] mixing,[6–8] and aero-acoustics.[9,10] Most work on turbulent jets is experimental. The direct numerical simulation (DNS) of spatially evolving turbulent jets is relatively recent. Boersma, Brethouwer, and Nieuwstadt[11] have performed one of the early DNS to study the dependence of the far-field self-similarity on inflow conditions. Lubbers, Brethouwer, and Boersma[12] extended this work to study the self-similarity of a passive scalar field in the turbulent jet. A direct computation of a turbulent compressible jet and its associated sound was performed by Freund, Lele, and Moin,[13] who also used their results to study the effect of compressibility on passive scalar mixing.[14] More recently, Pantano, Sarkar, and Williams[15] performed DNS with chemical reactions to study the mixing of a conserved scalar in nonpremixed turbulent combustion. DNS was used by Freund and Moin[16] to study the effect of pulsed blowing normal to a jet's shear layer near the jet exit.

Jets entrain free-stream fluid as they grow downstream. As a result simulations of spatially evolving jets allow for entrainment from the lateral boundaries. For example, Boersma, Brethouwer, and Nieuwstadt[11] use "traction-free" boundary conditions to enable entrainment at the lateral boundaries in their incompressible DNS. Freund *et al.*[13,16] use "sponge" boundary conditions at the lateral boundaries in their compressible DNS to prevent reflection of acoustic waves from the boundaries. These "nonreflecting" boundary conditions also serve to gently damp lateral entrainment from the near-field of the jet to the far-field. None of these numerical computations allow the jet to entrain fluid as it immediately exits the nozzle. Figure 1 shows a schematic of the effect of inflow entrainment on the streamlines in the jet near-field. Entrainment is thus expected to increase the axial momentum of the free-stream in the near-field.

The importance of inlet conditions on the development of axisymmetric jets is well-documented.[5,17–19] Apparently small changes at the inlet can significantly affect the subsequent evolution of the jet. The objective of this paper is to study the effect of inflow entrainment in simulations of spatially evolving jets. The paper is organized as follows. Section II discusses the use of a buffer region to allow inflow entrainment in the DNS, the numerical method, computational grid, and jet parameters. The effect of inflow entrainment on laminar jets is discussed in Sec. III A which compares the DNS to analytical solution. Section III B presents results for a turbulent jet, with comparison to experiment. A short summary in Sec. IV concludes the paper.

II. SIMULATION DETAILS

The governing equations are the incompressible Navier–Stokes equations:

$$\frac{\partial u_i}{\partial t} + \frac{\partial u_i u_j}{\partial x_j} = -\frac{1}{\rho}\frac{\partial p}{\partial x_i} + \nu\frac{\partial^2 u_i}{\partial x_j \partial x_j}, \quad \frac{\partial u_i}{\partial x_i} = 0, \tag{1}$$

where u_i, p, ρ, and ν denote the velocity, pressure, density, and kinematic viscosity, respectively. DNS was performed with and without inflow entrainment, at Reynolds numbers of 300 and 2400. Note that the jet is laminar at Re=300 and turbulent for Re=2400. All computations used unstructured grids of hexahedral elements. Figure 2 shows a schematic of a radial cross section. Note that the computational domain extends upstream of the jet exit for the simulations that allow inflow entrainment. This region is termed the "inflow buffer"

[a)]Author to whom correspondence should be addressed. Telephone: 612 624 4175; fax: 612 626 1558; electronic mail: mahesh@aem.umn.edu

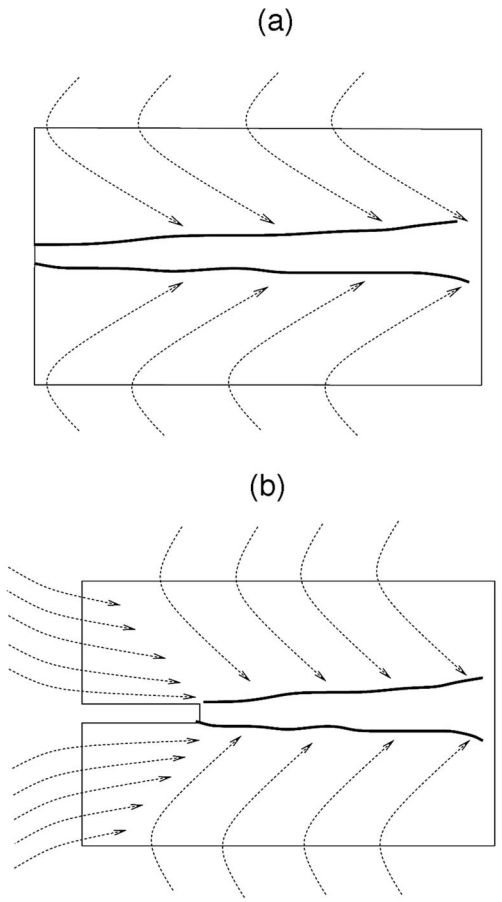

FIG. 1. Illustration of entrainment in jet (a) from lateral boundaries alone and (b) from lateral and inflow boundaries.

region. Simulations with the buffer region model the experimental situation where the jet exits a nozzle, located near the center of the room.

The numerical algorithm is described in detail by Mahesh, Constantinescu, and Moin[20] and will only be summarized here. The algorithm is a predictor-corrector formulation that emphasizes discrete energy conservation for the convection and pressure terms on unstructured grids with arbitrary elements. The Cartesian components of velocity and pressure are stored at the centroids of the grid elements, and face-normal velocities are stored at the centroids of the faces. The nonlinear and viscous terms are used to obtain a predictor value for the cell-centered velocities. The predicted values of u_i are used to obtain predicted values for the face-normal velocities, which are then projected to obtain the pressure. Once the pressure is obtained, the Cartesian velocities are updated using a least-squares formulation for the pressure gradient. Time advancement is explicit and uses the second-order Adams Bashforth method. The algorithm has been validated for a variety of turbulent flows by Mahesh, Constantinescu, and Moin,[20] and shown to be nondissipative yet robust, at high Reynolds numbers in very complex geometries.

Figure 2 shows a cross section of the computational domain. A top-hat velocity profile is specified at the jet exit (inflow), and no slip boundary conditions are specified at the lateral boundaries. Zero normal derivative boundary conditions are specified at the outflow to allow unsteady disturbances to exit the domain. The outflow boundary conditions also allow entrainment at the outflow boundary without compromising numerical stability. The laminar simulations extend to 25 jet diameters axially, 50 diameters radially, and use $\approx 1.2\times 10^6$ elements. The turbulent simulations extend to

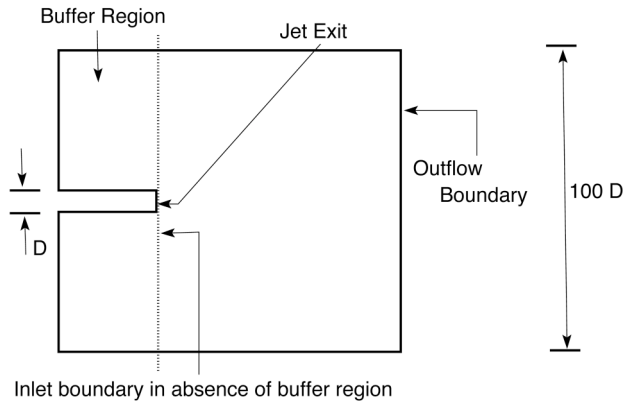

FIG. 2. Schematic of the computational domain. A radial cross section is shown.

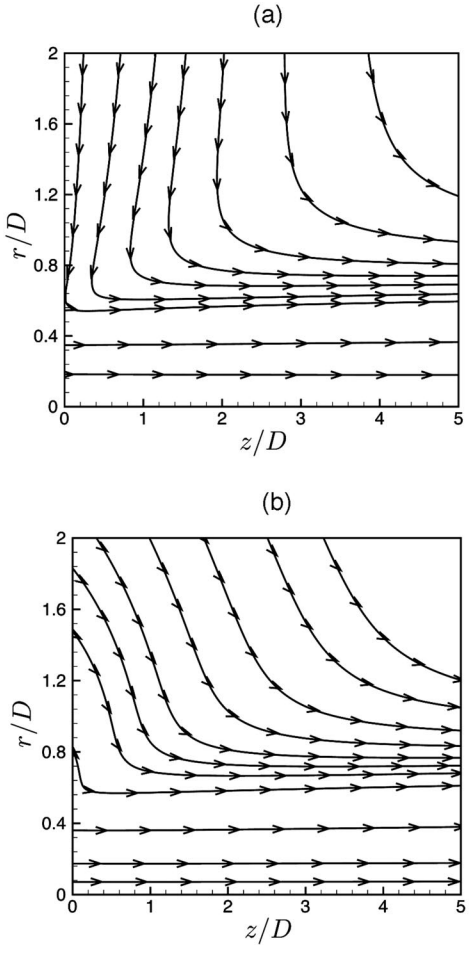

FIG. 3. The effect of inflow entrainment on streamlines near the jet exit at Re=300. A radial cross section is shown. (a) Without inflow entrainment and (b) with inflow entrainment.

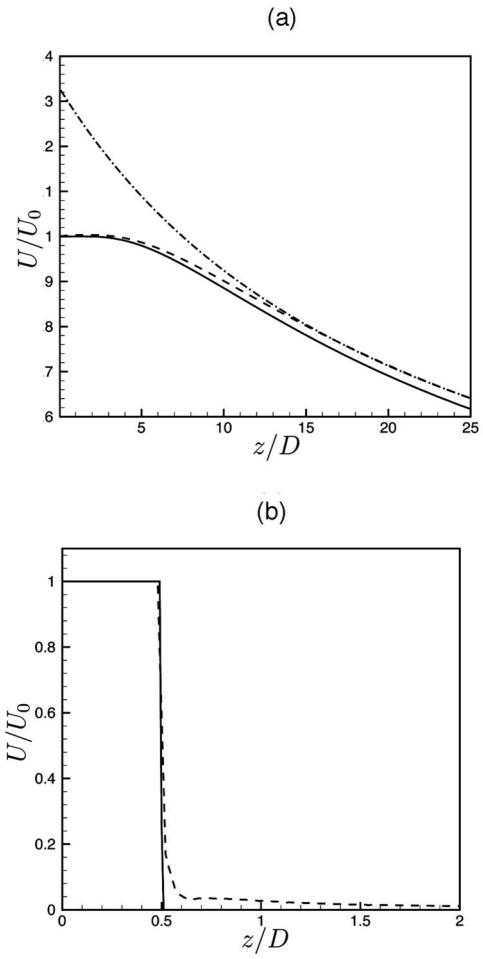

FIG. 4. (a) The axial velocity at the centerline of the Re=300 jet is compared to analytical solution. (– – –) Analytical solution (Ref. 22), (----) with inflow entrainment, (—) without inflow entrainment. (b) The effect of inflow entrainment on the axial velocity at the jet exit. (—) Without inflow entrainment and (----) with inflow entrainment.

50 jet diameters axially and 50 diameters radially. The simulations without the inflow buffer use $\approx 3.2\times10^6$ elements, while the simulations with the buffer region use 3.8×10^6 elements. The buffer region for the laminar jet extends 20 diameters upstream of the jet exit plane and 15 diameters for a turbulent jet.

The impact of radial confinement, and length of the buffer region were examined in detail for the Re=300 jet. The length of the buffer region was varied from 5D to 30D, and the solution was found not to change for lengths greater than 20D. Similarly, the jet was simulated for three radial extents of 20D, 30D, and 50D, respectively. The self-similar velocity profile for the 20D domain deviated from the analytical solution by approximately 5%, while the 30D and 50D domains agree with each other, and analytical solution. The use of unstructured grids allows the larger domains to be simulated at little additional cost. The grids are rapidly coarsened in the radial direction and in the axial direction upstream of the jet exit. For example, the grid size increases from 1.03×10^6 elements for the 30D radial domain to 1.17×10^6 elements for the 50D radial domain; i.e., the radial extent increases by 67% while the mesh size increases

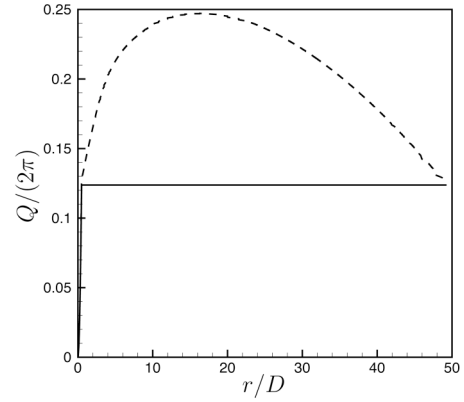

FIG. 5. Radial profile of volumetric flow rate at the jet exit for the Re =300 jet. (—) Without inflow entrainment and (----) with inflow entrainment.

only by 13.6%. Similarly, there is negligible increase in cost due to the buffer region; the increase in grid size due to the buffer is a modest 5.1% for the longest buffer considered. These observations were used to determine the domain sizes used for the reported simulations.

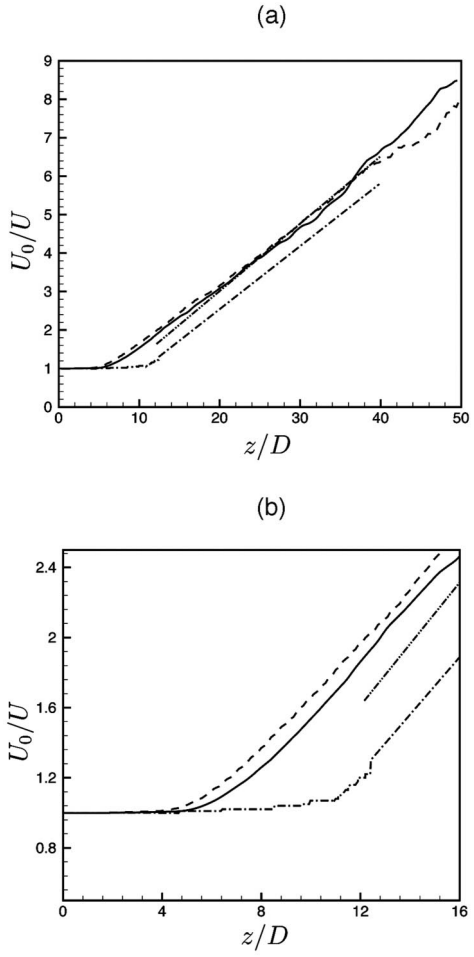

FIG. 6. Mean axial velocity at jet centerline as a function of distance from jet exit plane for the Re=2400 jet. (a) Entire domain, (b) near-field. (—··—) Wygnanski and Fiedler (Ref. 1), (– – –) Boersma *et al.* (Ref. 11), (----) present DNS with inflow entrainment, and (—) present DNS without inflow entrainment.

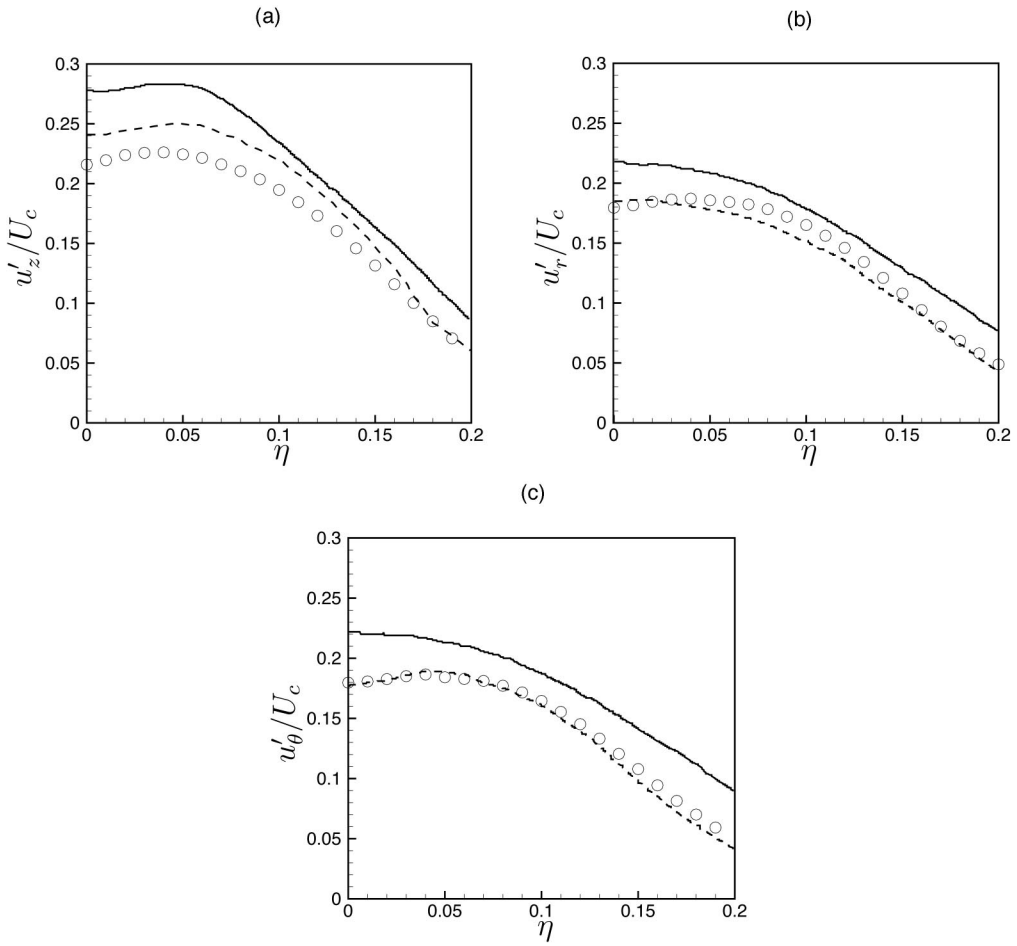

FIG. 7. Comparison of DNS results to experiment. The turbulence rms velocities scaled with local centerline velocity are plotted in similarity coordinates, $\eta = r/(z-z_0)$. (—) Hussein *et al.* (Ref. 3), (----) Panchapakesan and Lumley (Ref. 2), (○) present DNS. (a) Axial, (b) radial, and (c) azimuthal components.

III. RESULTS

A. Laminar jet at Re=300

The effect of inflow entrainment on laminar jets was studied for two inflow velocity profiles: top-hat and parabolic. DNS were performed with and without the buffer region. The effect of inflow entrainment was seen to be similar for both profiles. Only results for the top-hat profile are therefore shown here. Figure 3 shows an axial cross section of the jet near the jet exit with and without the buffer region. Note that the streamlines near the jet exit are significantly different in the presence of the buffer region. The streamline pattern in Fig. 3(b) is similar to that predicted by analytical solution for a steady jet originating from a point source of momentum (Ref. 21 and Fig. 4.6.1 therein). Note that accounting for inflow entrainment by providing the buffer region produces an effective co-flow free near the jet exit. Figure 4(a) compares the centerline axial velocity decay to analytical solution,[22]

$$U(r,z) = \frac{3K}{8\pi\nu(z-z_0)}\left(1 + \frac{3K}{64\pi\nu^2}\left(\frac{r}{z-z_0}\right)^2\right)^{-2}, \qquad (2)$$

where z_0 is the virtual origin of the jet, r denotes the radial distance from the jet centerline, and K is the momentum supplied by the point source at $z=z_0$. The solution obtained with inflow entrainment shows better agreement with the analytical solution. The radial profile of the axial velocity at the jet exit is shown in Fig. 4(b). Note that the axial velocity decreases rapidly away from the jet exit. In the absence of the buffer region, the axial velocity is zero for $r \geqslant D/2$. However, when the buffer region is present, the axial velocity is nonzero; e.g., it is 2.8% of the orifice velocity at a radial distance of a jet diameter from the centerline. This results in an effective co-flow. The volumetric flow rate in the plane of the jet exit, $Q(r) = 2\pi\int_0^r Ur'dr'$, is shown in Fig. 5. Note that $Q(r)$ is noticeably higher near the jet exit, when the jet entrains from upstream. The momentum on the jet exit plane was also computed. It was observed that the difference due to presence of the inflow buffer region is not as significant as seen for the volumetric flow rate. This is because axial velocity drops rapidly for $r > D/2$ and the momentum has a U^2 dependence on this axial velocity.

B. Turbulent jet at Re=2400

The turbulent simulations were initialized with a pseudorandom velocity field whose amplitude was 0.1% of the top-hat jet exit velocity U_0. Explicit time advancement was used with time step, $\Delta t \sim 0.008 D/U_0$. The simulations were run for $\approx 1200 D/U_0$ to allow initial transients to exit the

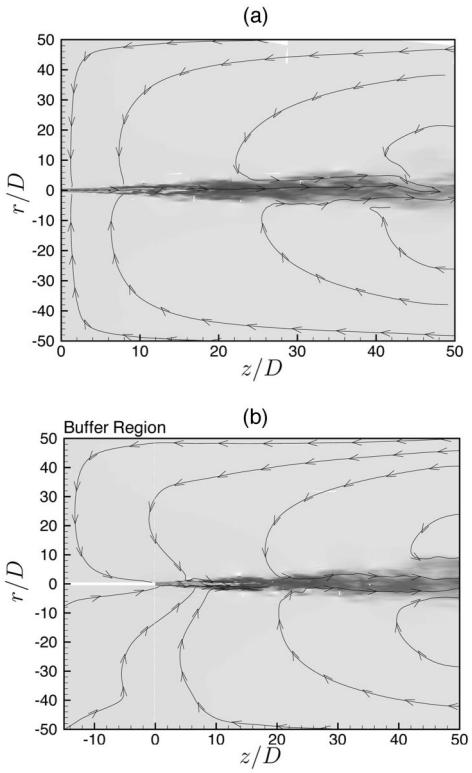

FIG. 8. The generation of an effective co-flow by inflow entrainment for the Re=2400 jet. (a) Without inflow entrainment and (b) with inflow entrainment.

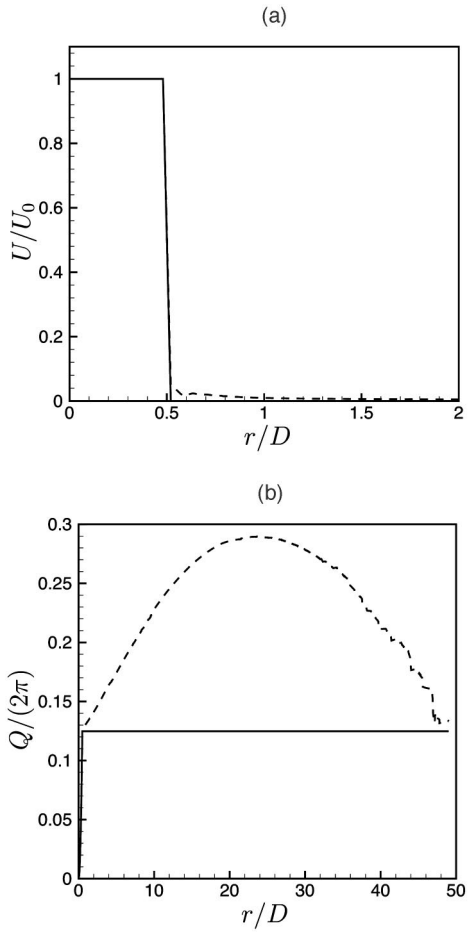

FIG. 9. (a) The effect of inflow entrainment on the axial velocity at the jet exit for the Re=2400 jet. (b) Volumetric flow rate at the jet exit for the Re=2400 jet. (—) Without inflow entrainment and (----) with inflow entrainment

domain. Statistics were gathered over the next $900D/U_0$ time units. The simulations are compared to the numerical simulations of Boersma, Brethouwer, and Nieuwstadt,[11] and Lubbers, Brethouwer, and Boersma,[12] and experimental data of Wygnanski and Fiedler,[1] Panchapakesan and Lumley,[2] and Hussein, Capp, and George.[3] Figures 6(a) and 6(b) show the decay of mean axial velocity with and without inflow entrainment at the jet centerline. Good agreement with experimental data is seen. Note that the simulation data from Ref. 12 show the core closing around $10D$ while the present simulations show the core closing between $4D$ and $5D$. This difference is attributable to two factors—smaller radial domain in simulations[12] ($\approx 4D$), and the absence of inflow entrainment in their computations. Note that Lubbers, Brethouwer, and Boersma[12] focus on the self-similar properties of the jet which are unaffected by the longer potential core.

Figures 7(a)–7(c) show the three components of turbulent intensities in similarity coordinates $\eta = r/(z-z_0)$. The DNS is compared to curve fits given in Refs. 2 and 3. The similarity profiles are obtained by averaging profiles over $15D \leqslant z \leqslant 40D$. Good agreement with Panchapakesan and Lumley[2] is seen, particularly for the radial and azimuthal velocities. The axial intensities in Fig. 7(a) seem to be lower at the jet centerline, but the difference between the DNS and results from Panchapakesan and Lumley[2] is less than the difference between the two experiments, themselves.

Instantaneous streamlines in a radial cross section are shown in Fig. 8, where the effect of inflow entrainment is similar to that observed for the laminar jet. The effective co-flow due to entrainment affects the length of the potential core. Figure 6(b) shows the mean axial velocity at the jet centerline. Note that the potential core closes a jet diameter earlier ($4D$ as compared to $5D$) when inflow entrainment is accounted for. The magnitude of the effective co-flow is shown in Figs. 9(a) and 9(b), respectively, where radial profiles of the mean axial velocity, and the volume flow rate $Q(r) = 2\pi \int_0^r U r' dr'$ are evaluated at the jet exit. In the presence of inflow entrainment, the flow rate increases monotonically till $r \sim 20D$ and then starts decreasing when the reverse flow in the free stream becomes predominant. Note that $Q(r)$ increases to a maximum of 130% of the flow rate in the jet nozzle due to inflow entrainment.

These differences in the mean velocity affect the turbulence intensities in the near-field. In particular, the region around the closing of the potential core is strongly intermittent, and hence characterized by high turbulent intensities. This region is known to significantly influence jet properties such as the emitted sound. Figure 10 shows the effect of inflow entrainment on the axial turbulent intensity and rms value of pressure. Note that the highest intensities are around the region where the potential core closes. The turbulent velocity and pressure fluctuations both peak about a diameter

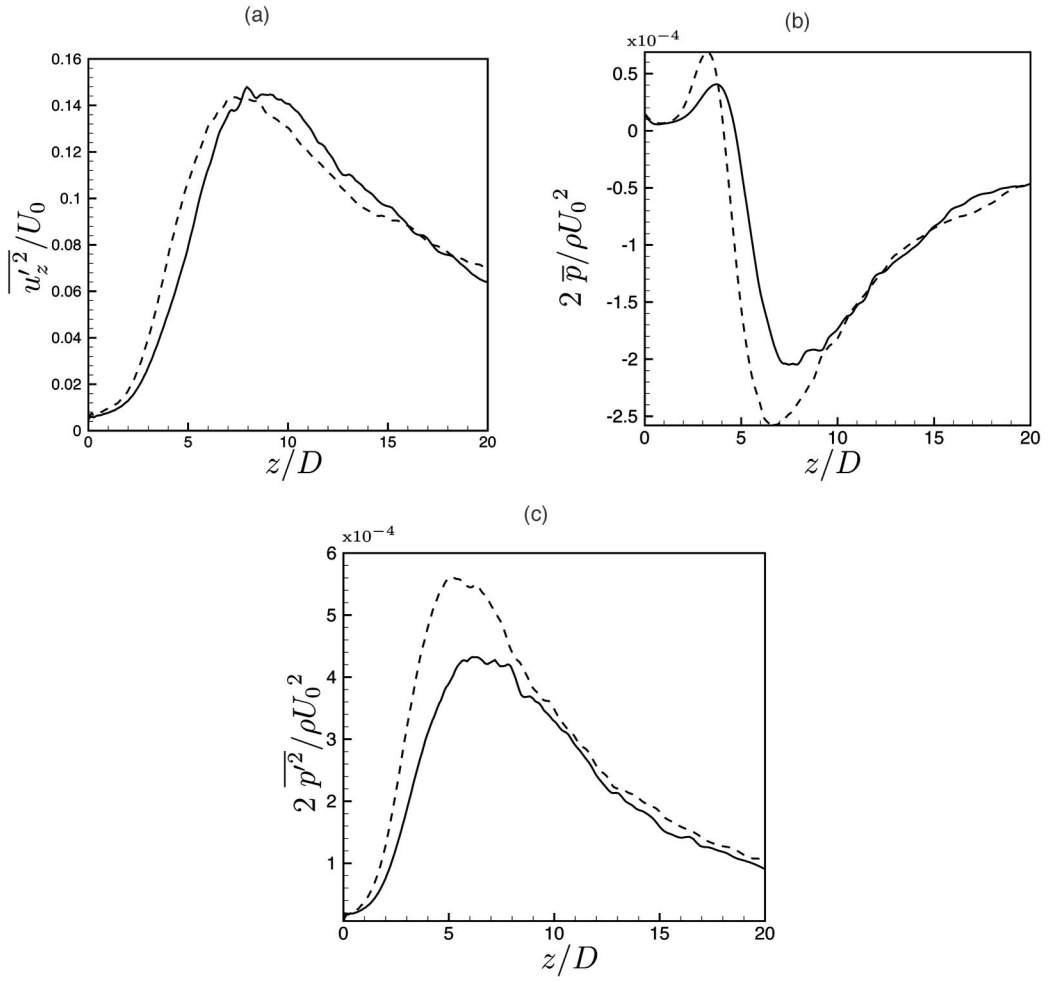

FIG. 10. The effect of inflow entrainment on the turbulent velocities and pressure fluctuations in the near-field of the Re=2400 jet. (a) Axial turbulence intensities scaled with local centerline velocity, (b) mean pressure scaled with jet exit velocity, (c) rms pressure fluctuations scaled with jet exit velocity. (—) Without inflow entrainment and (----) with inflow entrainment.

upstream in the presence of inflow entrainment. This behavior is consistent with the fact that jet core closes about a jet diameter earlier (Fig. 6) due to the presence of buffer region. The peak levels of pressure fluctuations are seen to be higher in the presence of the buffer region, while the peak levels of the axial turbulent velocity are seen to be the same. The observed behavior of the axial turbulent fluctuations is consistent with experimental measurements in co-flowing jets (e.g., Sadr and Klewicki[23]) which show that turbulent intensity levels of velocity do not change appreciably when the velocity ratio between inner and outer jet is varied.

IV. SUMMARY

Direct numerical simulations were performed for a laminar (300) and turbulent (2400) jet. The importance of accounting for entrainment near the jet exit was shown. This entrainment can be realized by providing an inflow buffer region upstream to the jet exit plane. Results were presented for a laminar and turbulent jet, with and without the buffer region. Inflow entrainment was shown to produce an effective co-flow which significantly increases the volume flow rate near the jet exit in the free stream. The potential core is seen to close earlier in the presence of inflow entrainment. As a result, near-field turbulent intensities and pressure fluctuations on the jet centerline are noticeably affected. When plotted in similarity variables, the far-field solutions with and without inflow entrainment agree well with each other and experiments. The results suggest the importance of allowing for inflow entrainment in simulations of turbulent jets, particularly for studies where near-field behavior is important.

ACKNOWLEDGMENTS

We are grateful to the Department of Energy for their financial support through the Stanford ASCI Alliance Program, Computing time was provided by the Minnesota Supercomputing Institute and the San Diego Supercomputer Center.

[1] I. Wygnanski and H. E. Fiedler, "Some measurements in the self preserving jet," J. Fluid Mech. **38**, 577 (1969).
[2] N. R. Panchapakesan and J. L. Lumley, "Turbulence measurements in axisymmetric jets of air and helium. Part 1. Air jet," J. Fluid Mech. **246**, 197 (1993).
[3] H. J. Hussein, S. P. Capp, and W. K. George, "Velocity measurements in a high Reynolds number, momentum-conserving axisymmetric turbulent jet," J. Fluid Mech. **258**, 31 (1994).

[4]E. J. Gutmark and F. F. Grinstein, "Flow control with non-circular jets," Annu. Rev. Fluid Mech. **35**, 295 (1999).
[5]W. C. R. Reynolds, D. E. Parekh, P. J. D. Juvet, and M. J. D. Lee, "Bifurcating and blooming jets," Annu. Rev. Fluid Mech. **35**, 295 (2003).
[6]R. E. Breidenthal, "Structure in turbulent mixing layers and wakes using a chemical reaction," J. Fluid Mech. **109**, 1 (1981).
[7]P. E. Dimotakis, "Mixing transition in turbulent flows," J. Fluid Mech. **409**, 69 (2000).
[8]Z. Warhaft, "Passive scalars in turbulent flows," Annu. Rev. Fluid Mech. **32**, 203 (2000).
[9]M. E. Goldstein, "Aeroacoustics of turbulent shear flows," Annu. Rev. Fluid Mech. **16**, 263 (1984).
[10]C. K. W. Tam, "Supersonic jet noise," Annu. Rev. Fluid Mech. **27**, 17 (1995).
[11]B. J. Boersma, G. Brethouwer, and F. T. M. Nieuwstadt, "A numerical investigation on the effect of the inflow conditions on the self-similar region of a round jet," Phys. Fluids **10**, 899 (1998).
[12]C. L. Lubbers, G. Brethouwer, and B. J. Boersma, "Simulation of the mixing of a passive scalar in a round turbulent jet," Fluid Dyn. Res. **28**, 189 (2001).
[13]J. B. Freund, S. K. Lele, and P. Moin, "Compressibility effects in a turbulent annular mixing layer. Part 1. Turbulence and growth rate," J. Fluid Mech. **421**, 229 (2000).
[14]J. B. Freund, "Noise sources in a low Reynolds number turbulent jet at Mach 0.9," J. Fluid Mech. **438**, 277 (2001).
[15]C. Pantano, S. Sarkar, and F. A. Williams, "Mixing of a conserved scalar in a turbulent reacting shear layer," J. Fluid Mech. **481**, 291 (2003).
[16]J. B. Freund and P. Moin, "Jet mixing enhancement by high-amplitude fluidic actuation," AIAA J. **38**, 1863 (2000).
[17]P. Bradshaw, "The effect of initial conditions on the development of a free shear layer," J. Fluid Mech. **26**, 225 (1966).
[18]A. J. Yule, "Large-scale structure in the mixing layer of a round jet," J. Fluid Mech. **89**, 412 (1978).
[19]D. Z. Husain and A. K. M. F. Hussain,"Axisymmetric mixing layer: influence of the initial and boundary conditions," AIAA J. **17**, 48 (1979).
[20]K. Mahesh, G. Constantinescu, and P. Moin, "A numerical method for large-eddy simulation in complex geometries," J. Comput. Phys. **197**, 215 (2004).
[21]G. K. Batchelor, *An Introduction to Fluid Mechanics* (Cambridge University Press, Cambridge, 1988).
[22]H. T. Schlichting, *Boundary Layer Theory* (McGraw-Hill, New York, 1979).
[23]R. Sadr and J. C. Klewicki, "An experimental investigation of the near-field flow development in coaxial jets," Phys. Fluids **15**, 1233 (2003).